1

DYNAMICS OF PHOTOCHEMICAL REACTIONS OF ORGANIC CARBONYLS AND THEIR CLUSTERS

DORIT SHEMESH[1] and R. BENNY GERBER[1,2,3]

[1]*Institute of Chemistry and the Fritz Haber Research Center, The Hebrew University of Jerusalem, Jerusalem, Israel*
[2]*Department of Chemistry, University of California, Irvine, CA, USA*
[3]*Laboratory of Physical Chemistry, University of Helsinki, Helsinki, Finland*

1.1 INTRODUCTION

Photochemical reactions are central to organic chemistry and are playing a key role in atmospheric aerosols [1]. A variety of reactions occur, and the majority of them involve more than one molecule, mostly surrounded by a cluster (e.g., water). A common approach in modeling is to simplify the system and to treat only unimolecular reactions [2, 3]. However, understanding the processes involved in cluster is of great interest itself and approaches for modeling those processes need to be developed.

Theoretical simulation of photochemistry of organic molecules in clusters is very complicated and challenging due to the following reasons. The size of the system usually is too large for the usage of quantum chemistry–based methods. Condensed phase systems are commonly treated using classical mechanics [4]. On the contrary, force-field potentials utilized for large systems are not applicable here, since those are unable to treat reactions at all. Additional complications arise from the lack of potential energy surfaces for open shell systems, as well as the correct treatment of nonadiabatic transitions between different surfaces. The objective of this chapter is to provide theoretical tools for describing photochemical reactions of organic molecules in clusters and in condensed phase. The chapter focuses on the modeling of photochemical organic reactions using on-the-fly molecular dynamics on a semiempirical potential energy surface. It will be shown that semiempirical methods have the great advantage of being computationally fast enough and simultaneously provide qualitatively an accurate enough description of the systems.

Advances in Chemical Physics, Volume 159, First Edition. Edited by Paul Brumer.

An additional objective of this chapter is to provide mechanistic details and timescales for the important class of reactions in organic carbonyls. Organic carbonyls are of interest due to their importance in atmospheric chemistry and related areas [1, 5–7]. Carbonyls are important in addition to atmospheric chemistry in combustion, petroleum chemistry, biochemistry, and food chemistry. In several of these, the issue of photochemistry/photostability arises. Mechanistic details are known currently for relatively small carbonyls, as seen in the work by [8–30]. Large molecules are challenging for the simulation.

Pentanal, an aliphatic aldehyde, has been chosen for representing the unimolecular reactions of carbonyls [31, 32]. *cis*-Pinonic acid has been chosen as a representative ketone [33]. The abundance of carbonyl compounds in the atmosphere is very high. Certain carbonyls are directly emitted by various sources, but the vast majority of them are produced in the atmosphere by oxidation of hydrocarbons [1]. Photolysis serves as an important removal pathway for atmospheric carbonyls. In the lower atmosphere, where the availability of radiation is limited to wavelength above ~290 nm, the photolysis of carbonyls is driven by their weak absorption band in the wavelength range of 240–360 nm as a result of a dipole-forbidden $n \rightarrow \pi^*$ transition [1, 34]. Photolysis of aldehydes, such as pentanal, is known to occur through the following pathways:

$$\begin{aligned} \mathrm{RCHO} + \mathrm{h}\nu &\rightarrow \mathrm{RH} + \mathrm{CO} && \text{(A)} \\ &\rightarrow \mathrm{R} + \mathrm{HCO} && \text{(B)} \\ &\rightarrow \mathrm{R''} = \mathrm{R'} + \mathrm{CH_3CHO} && \text{(C)} \\ &\rightarrow \mathrm{RCO} + \mathrm{H} && \text{(D)} \end{aligned}$$

Process A is the molecular fragmentation channel. Process B represents the fragmentation into two free radicals (Norrish type I splitting). Process C is called a Norrish type II splitting, and it results in acetaldehyde and an alkene as the products. Norrish type II splitting is only possible for aldehydes larger than butanal, and the reason pentanal was selected as the model for this work is to make sure this important channel is included in the calculation. Process D is an H abstraction process and has been found to be minor in small aldehydes [35]. In the microscopic picture, the photoexcitation promotes the system to the first excited singlet state (S_1) of $n\pi^*$ character. The S_1 state can either switch to the ground S_0 state via internal conversion (IC) or reach the lowest triplet state T_1 via intersystem crossing (ISC). There is evidence that process B can occur either on the ground state or on the triplet state [36]. Reactions for ketones differ in part, but the two types of mechanisms are related, and both involve Norrish processes.

The above processes describe the possible unimolecular reactions occurring after photoexcitation of aldehydes. For assessing the effect of solvation on the photochemistry, the following model systems have been used. Pinonic acid has been studied with one and five water molecules, and a pentanal cluster using five identical pentanal molecules has been built.

The structure of this chapter is as follows: Section 1.2 provides an overview of the methodological approach of this study, in particular with emphasis on providing supporting validation for the semiempirical method. Section 1.3 gives results and discussion and finally Section 1.4 summarizes conclusions.

1.2 METHODOLOGY AND SYSTEMS

The simulation of the photoexcitation process has been done here using on-the-fly molecular dynamics on a semiempirical potential energy surface. In brief, the first step involves molecular dynamics on the singlet ground state at 300 K. From this run, excitation from selected geometries to the singlet excited state occurs. After a short run on the singlet excited state, surface structures with a small S_1–T_1 gap are chosen. Those are used as starting geometries for the triplet state molecular dynamics simulation. In some of the simulation, the molecular dynamics simulation on the singlet state surface is omitted. For a detailed description and justification of this approach, the reader is referred to Section 1.2.3 and Refs [31, 33, 37].

Here we first discuss, in Section 1.2.1, the potential energy surface employed in this simulation. In Section 1.2.2, we discuss on-the-fly molecular dynamics approach. The different steps of the excitation process itself are explained in Section 1.2.3. The systems used are described in Section 1.2.4.

1.2.1 Potential Energy Surfaces

As already discussed in the introduction, the two edges regarding the accuracy of potential energy surfaces are (i) computationally very demanding high-level quantum methods for relatively small systems yielding very accurate data and (ii) comparable cheap force-field-based potential energy surfaces for very large systems (e.g., proteins) yielding qualitative information of nonreactive processes. In some cases of photochemical processes in condensed phases, *ad hoc* empirical potentials were constructed that seem to offer a reasonable description of the process [4]. However, in general, this does not seem a practical approach. Since the simulation of the processes required on the one hand potentials capable of describing reactions and on the other hand computational cheap ones, the choice has fallen on semiempirical methods. Semiempirical methods have been derived from the Hartree–Fock method and are therefore close to quantum methods [38]. Integrals are simplified by using parameters adapted to experimental data (e.g., heat of formation) and are therefore calculated very fast. Thus, semiempirical methods are capable of providing mechanistic information on photochemical processes in a relatively short time and are able to treat medium-size systems in a reasonable time.

The semiempirical method used in this study is the OM2/MRCI method developed by Thiel and coworkers [39, 40]. In the OM2 method, proper orthogonality of the orbitals has been introduced, which leads to a better description of energy

barriers between different conformers. This method has been already applied to a great success in several studies by our group [31–33, 41, 42]. Other previously applied semiempirical method used in similar studies of our group is PM3 on modeling the vibrational spectra and the dynamics of relevant organic systems [37, 43–49]. All those studies have established semiempirical methods as a reliable tool.

All of the systems were initially optimized using a much higher level of theory, in order to ensure that the OM2 method provides a realistic description of the structure. The method employed was the second-order Møller–Plesset perturbation theory (MP2) [50] using the cc-pVDZ basis set [51]. The resolution-of-identity (RI) approximation for the evaluation of the electron-repulsion integrals implemented in Turbomole was utilized [52].

The advantage of the OM2 semiempirical method compared to other forms of approximations of related semiempirical methods lies in the ability of treating excited states and open shell systems. Excited states can be calculated using the OM2/MRCI variant of this method [40]. In this variant, an active space of orbitals is chosen, similar to a CASSCF calculation. In addition, different reference wave functions are employed and excitations from these reference functions are allowed. With this method, multireference systems can be treated by using several configurations for a particular state. For additional validation of the semiempirical method, the excitation energies were calculated by using the algebraic diagrammatic construction method 2 (ADC(2)) [53]. The semiempirical methods OM2 and OM2/MRCI are available in the semiempirical MNDO program [54].

For the photochemistry of organic carbonyls, several potential energy surfaces are important. First, excitation occurs from the singlet ground state potential energy surface. Accurate description of the ground state potential energy surface using the semiempirical OM2 method is ensured through comparison to the MP2 energies and structures for the same system (see Section 1.3.1 for further details). Second, correct description of the first singlet excited state is very important, since initial excitation occurs to this surface. Therefore, this surface is validated against higher level electronic structure methods such as ADC(2); see Section 1.3.1 for further explanation. In the next step, ISC is assumed to occur from S_1 to T_1. Experimental evidence supports the occurrence of the reactions on the triplet state surface [36]. In addition, for the pentanal molecule, the region of the ISC is obtained by investigation of all the relevant singlet and triplet state surfaces along the C—C_α cleavage coordinate using the semiempirical potential energy surface OM2/MRCI, as well with the ADC(2) method. It can be concluded from the relevant curves (see Ref. [31]) that the ISC region is indeed near the Franck–Condon region of initial excitation and therefore can be reached with a high probability.

In addition, we have tested for the possibility of nonadiabatic transitions both between different singlet state surface and between different triplet state surfaces but have not found any sign for this.

1.2.2 On-the-Fly Molecular Dynamics

On-the-fly molecular dynamics have been employed in order to simulate the photochemistry of carbonyl-containing compounds. The on-the-fly mechanism implemented in the MNDO program is the velocity-Verlet algorithm. Here an additional aspect of the usage of a computational cheap semiempirical method is visible. In order to provide realistic relative yields of different photochemical reactions, a large enough sample of trajectories is needed. For these systems, a substantial amount of trajectories (around 100) has been calculated for a relatively long timescale (up to 100 ps).

1.2.3 Modeling of the Excitation Process

The simulation of the excitation process can be described by four main steps depicted in Figure 1.1. (i) MD simulation on the ground state for sampling of the initial configuration, (ii) vertical excitation of selected geometries and dynamics on the singlet excited state, (iii) assumption of ISC at the smallest singlet-triplet gap, and (iv) dynamics on the triplet ground state.

After reaching the first excited singlet state S_1, molecular dynamics simulations on this state have been pursued. Two different approaches were used: (i) molecular dynamics simulation only on the S_1 singlet state surface and (ii) molecular dynamics simulations using Tully's nonadiabatic surface hopping method, allowing transitions between different singlet excited states and the ground state [55]. The objective of this step was to determine whether reactions occur on the singlet excited state and whether different excited states contribute to the dynamics. The results on this were very clear: For the timescale simulated here, we have not observed reactions, and no transfer to other states happened. Due to these findings, this step (MD simulation on the singlet excited state, i.e., part of step 2) was omitted in further simulations of photochemical reactions. Experimental evidences

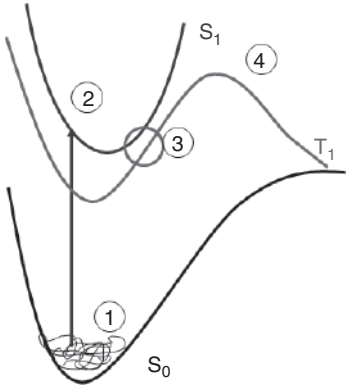

Figure 1.1 Schematic picture of the simulation approach. Numbers denote the sequence of steps involved. (1) MD simulation on the ground state. (2) Vertical excitation of selected geometries and dynamics on the singlet excited state. (3) Assumption of intersystem crossing at the smallest singlet-triplet gap. (4) Dynamics on the triplet ground state. Reproduced with permission from Ref. [31]. Copyright 2013 American Chemical Society.

also support the approach used here that the reactions are occurring on the triplet state surface [36]. In the initial approach, the identification of structures where the ISC take place, structures with the smallest energy gap between the S_1 and T_1 energy states were computed on structures from the MD simulation on the first excited state. This has been changed in later studies by selecting structures from the ground state molecular dynamics simulations and by calculation of the S_1–T_1 gap on these structures.

Also noteworthy is that we have also explicitly checked for nonadiabatic transitions between triplet states. In our simulation, we have not found any evidences for this.

In summary, first molecular dynamics simulation on the ground state potential has been carried out using the velocity-Verlet algorithm at 300 K with a time step of 0.1 fs for 10 ps. On those geometries, the S_1–T_1 gap was calculated. About 100 geometries with the lowest gap were chosen as initial geometries for the molecular dynamics simulation on the T_1 surface. The S_1–T_1 gap was in the average order of 0.5 eV. For the range of S_1–T_1 gap in the different systems employed here, the reader is referred to Refs [31, 33, 37]. The dynamics on the T_1 state was pursued for about 100 ps. The cleavage distance for describing bond breaking was set to 2.5 Å.

We would like to point out that the focus in these studies was on the mechanistic aspect and the timescale involved in the dynamics after the ISC event and not on the ISC event itself. For many organic compounds, the spin-flip dynamics is in general not ultrafast (timescale of ISC is in the order of 10^{-8} s) due to the weak spin-orbit couplings [56]. The long timescale involved makes it unfeasible to simulate the ISC event itself.

1.2.4 Systems

In our study, we have focused on several systems, which will be described shortly here. More information on the systems can be found in Refs [31–33].

1.2.4.1 Pentanal

Pentanal: The global minimum of pentanal is shown in Figure 1.2a. Pentanal is a five-carbon-long aldehyde and has been chosen for the following reason. The yields of Norrish type I and Norrish type II reactions strongly depend on the length of the chain. Aldehydes shorter than four carbon atoms tend to react primarily according to Norrish type I reaction due to the lack of an H atom at the C_γ-position. At the length of four carbon atoms, the Norrish type II process occurs with minor yield compared to the Norrish type I reaction. The length of pentanal is considered to be the turning point between both reactions: From this length on, the Norrish type II reaction is more pronounced.

Pentanal cluster: In order to study the effect of a cluster on the photochemical dynamics, a cluster of five pentanal molecules has been constructed. All the molecules have been aligned such that all carbonyl groups point to the same

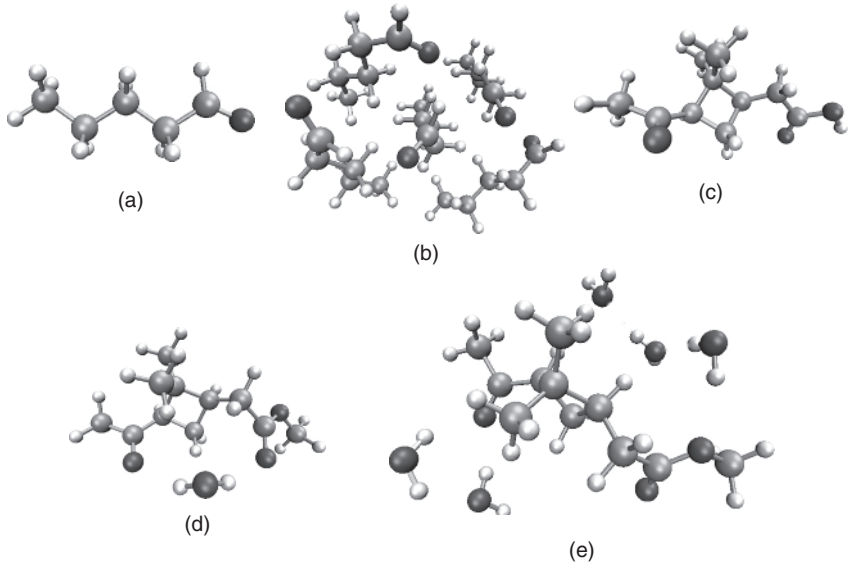

Figure 1.2 Optimized geometries of (a) pentanal, (b) pentanal cluster consisting of five pentanal molecules, (c) *cis*-pinonic acid, (d) methylated *cis*-pinonic acid with one water molecule, and (e) methylated *cis*-pinonic acid with five water molecules.

direction as can be seen in Figure 1.2b. For this cluster, dispersion forces are important, since otherwise, pentanal molecules start to evaporate. With dispersion forces included, the structure remains stable and does not change much during the simulation. Therefore, the state of the system can be described as "solid-like" rather than "liquid-like." The optimized structure might not represent the global minimum but corresponds to a reasonable choice of a low-energy minimum. The cluster size of five pentanal molecules was chosen due to the following considerations: First of all, the cluster is small enough to allow calculations using the semiempirical OM2/MRCI method. Second, the cluster is large enough to fully surround one pentanal molecule by additional pentanal molecules. Unimolecular reactions may be therefore significantly affected and cross-molecular reactions may be encouraged. Finally, the size of the cluster seems to be reasonable for future experimental studies. Noteworthy also in this context is the excitation process of the cluster itself: we assume that the excitation is localized on a single molecule, and it remains localized until the ISC to T_1.

1.2.4.2 Pinonic Acid (PA)

Pinonic acid: Pinonic acid involves a four-membered ring, which itself can undergo structural changes due to the photoexcitation. The structure of the molecule is depicted in Figure 1.2c.

Pinonic acid with one or five water molecules: The solvation of pinonic acid with water was modeled by using one or five water molecules; see Figure 1.2d and e, respectively. These provide relatively small cluster, which are still computationally feasible for applying molecular dynamics simulations. Case studies have shown that a single molecule already can affect the chemistry of a system dramatically. Simulation of the bare molecule and a cluster of one or five water molecules around pinonic acid should provide a trend for the effect of solvation on pinonic acid. On the hydrated system, calculations were done on for the *pinonic acid methyl ester* (PAMe). This substitution prevents the carboxyl group of PA from drawing water molecules away from the carbonyl group on the opposite end of the molecule, where photochemistry is initiated. As the main focus of this work is on the carbonyl-driven photochemistry of PA, the interactions of water molecules with the carboxyl group are of lesser interest. The carboxyl group is sufficiently isolated, and the PA → PAMe substitution should not have a strong effect on the photodissociation dynamics.

1.3 RESULTS AND DISCUSSION

1.3.1 Validation of the Semiempirical Method

So far, we have already pointed out the reasons for the choice of the semiempirical method for the description of the photochemistry in organic systems. In this section, we provide evidences for the validity of semiempirical methods, in particular the OM2 method employed in this context. The OM*x* potentials, in general, have been recently tested for thermochemistry, kinetics, and noncovalent interactions [57]. For organic molecules, the benchmark study shows that these methods are almost as accurate and robust as Density Functional Theory – Generalized Gradient Approximation methods for organic molecules. Several studies have employed the OM2/MRCI method in describing excited-state processes of organic molecules, for instance, nucleobases [58–64], butadiene [65], retinal model systems [66], and the rhodopsin chromophore [67]. These studies conclude that the description obtained by these potentials is reasonably good. Additional evidences come from the recent benchmark studies using OM2/MRCI, which show the good performance of the method [64, 68, 69]. And finally, the rich history of successful studies performed in our group using semiempirical methods, such as the photoionization dynamics of biological molecules, overtone excitation in atmospherically relevant systems, and vibrational excitation in small peptides, supports the choice of those methods [31, 32, 37, 42–49].

As can be seen in the studies mentioned above, prior to the massive usage of semiempirical methods in the production runs, a thorough validation against experiment or higher level *ab initio* method is necessary. The choice in our studies for validation purposes is the application of the well-established MP2 method for ground state structures and properties, and the usage of ADC(2) for excitation

energies, excited state structures, and properties. We strongly recommend those methods for validation purposes in organic systems.

1.3.2 Norrish Type I and Norrish Type II Reactions in the Isolated Molecule

Pentanal: As mentioned above, the photochemistry of pentanal is taking place on the triplet state. In this system, we have also checked whether reactions occur also on the singlet state. Therefore, as a first step before simulation, the potential energy surfaces (i.e., both vertical excitation to excited singlet states and ground and excited triplet states) were computed using OM2/MRCI and compared to ADC(2). It has been found out that the potential energy surfaces are qualitatively and quantitatively well described by OM2/MRCI. The interested reader is referred to Ref. [31] for more information. Three different pathways have been observed in the molecular dynamics simulation on the triplet state surface. In this section, we focus on Norrish type I and II reactions. The H detachment pathway is described in more detail in Section 1.3.3. In particular, for Norrish type I reaction, the first step, namely, the C—C_α cleavage, is observed in the simulation. The major pathway obtained in this simulation is the first step of Norrish type II reaction: H transfer from the H connected to the C_γ to the carbonyl group. Table 1.1 summarizes the yield of these reactions at a temperature of 300 K for the timescale of 100 ps. The yields of these reactions at a shorter timescale of lower temperature ($T = 200$ K) is discussed in Ref. [31]. Comparing shorter timescales versus longer timescales reveals that Norrish type II channel does not open immediately in the beginning but opens up only much later (after the first 10 ps).

Table 1.1 clearly shows that the major pathway in the photochemistry of pentanal is the γ-H transfer, followed by the C—C_α cleavage. The H detachment is only a minor pathway. A high percentage of trajectories are unreactive in this timescale. The relative yield of Norrish type I versus Norrish type II reaction from this table is 66% Norrish type II reaction and 34% Norrish type I reaction. This compares well to the observed experimental yield of 80% for Norrish type II reaction [16, 70].

TABLE 1.1
Percentage of Observed Reactions at $T = 300$ K for the Timescale of 100 ps

Pathway	Percentage of Observed Reactions
C—C_α cleavage	14
γ-H transfer	27
H detachment	1
Unreactive trajectories	58

Mechanistic details on Norrish type I and Norrish type II reactions are fully discussed in Ref. [31]. These include a detailed discussion about bond order and Mulliken charges along the two sample trajectories of Norrish type I and II. Validation is added for the Norrish type I trajectory by comparing the OM2/MRCI orbitals by those obtained by ADC(2). We focus here only on qualitative insight on these reactions. Figure 1.3 shows snapshots of the first step in the Norrish type I reaction, C—C_α cleavage. The step itself does not involve major rearrangements of the structure and does therefore occur very quickly. C—C_α cleavages are already observed in the first 10 ps, a timescale, where Norrish type II hardly occurs.

To compare with, Figure 1.4 shows the first step of the Norrish type II reaction, namely, the γ-H transfer to the C═O group.

The snapshots show various configurations along the dynamics. Initially, the γ-H is far away from the carbonyl group. The system has to reach the right configuration for the γ-H transfer. Therefore, the timescale of this process is much longer than for the simple C—C_α cleavage. Because of this, most of the trajectories reach first the cleavage of the C—C_α bond. In the gas phase, both fragments separate from each other. In the solvent, the reaction might be different, due to the surrounding molecules. This is discussed in Section 1.3.5. Additional investigation of the potential energy surfaces for Norrish type II process reveals that the energy after the H transfer is much lower than the energy before, suggesting a stabilization of the newly created structure compared to the initial isomer.

The comparison timescale of the Norrish type I versus Norrish type II reactions is very interesting and is summarized in the histogram in Figure 1.5.

Norrish type I reaction occurs on two timescales; one is ultrafast and below 10 ps and the second is slower at 45 ps. On the other hand, Norrish type II reaction

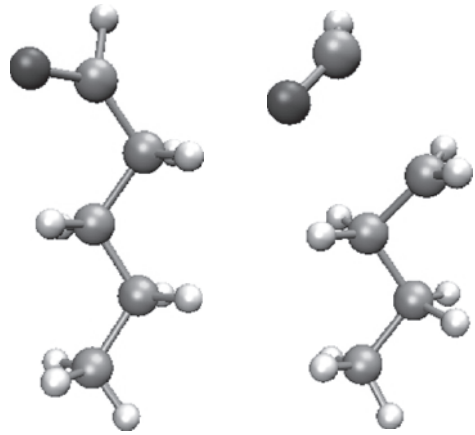

Figure 1.3 Pentanal: Snapshots of C—C_α cleavage. Reprinted with permission from Ref. [31]. Copyright (2013) American Chemical Society.

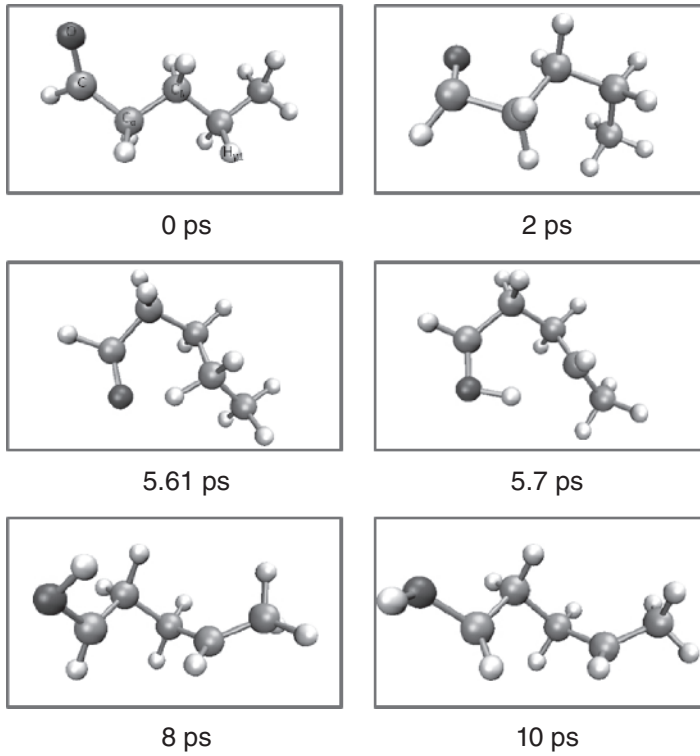

Figure 1.4 Pentanal: Snapshots of γ-H transfer. Reprinted with permission from Ref. [31]. Copyright (2013) American Chemical Society.

does start only after 20 ps. The following interpretation suggests an explanation for the differences in timescales and yields of the Norrish reactions. From a structural point of view, the C—C_α cleavage is much simpler than the structural rearrangement needed for the H transfer. In addition, the dissociation energy for the C—C_α cleavage is lower than for the C—H cleavage. However, the C—H cleavage of Norrish type II reaction occurs simultaneously with a new bond formation, which lowers the energy barrier for the whole process. This is also supported by the ΔH computed in Ref. [16], favoring Norrish type II process. Therefore, the yield of Norrish type II reaction is higher than Norrish type I reaction.

Another important effect on the Norrish type I/II ratio is the occurrence of intramolecular vibrational energy redistribution (IVR). For short timescale processes shorter than 10 ps (such as the Norrish type I reaction), IVR is yet far from completed as assumed by statistical theories such as RRKM. The opposite is true for Norrish type II reaction. The reaction only starts after 20 ps, pointing out that IVR seems to be necessary for the reaction. The longer the carbon chain (the larger

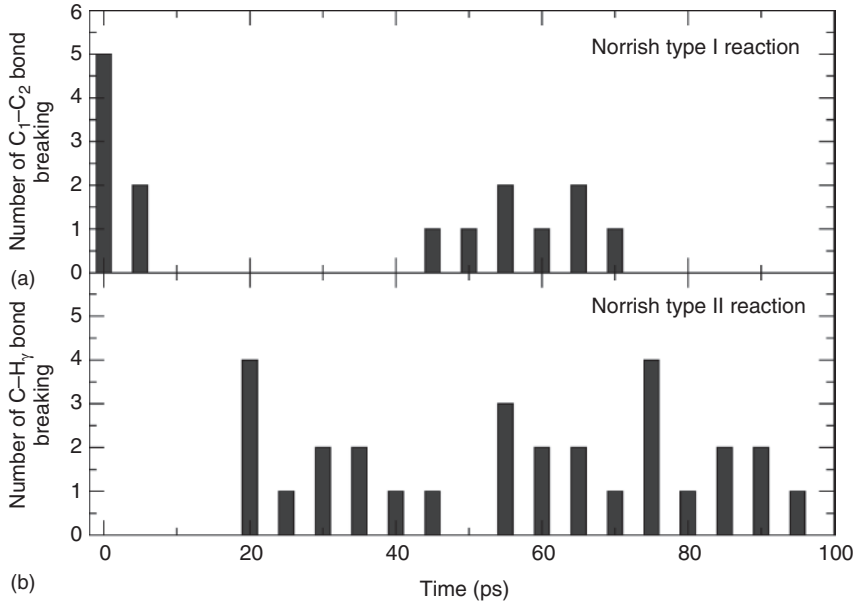

Figure 1.5 Histogram of (a) Norrish type I reactions and (b) Norrish type II reactions in Pentanal in the timescale of 100 ps. Reprinted with permission from Ref. [31]. Copyright (2013) American Chemical Society.

the system), the more IVR is expected. Thus for larger aldehydes, more Norrish type II reaction is predicted.

Finally, the discrepancy between experiment and theory on the ratio between Norrish type I reaction and Norrish type II reaction can be explained by considering the following factors. Experimental conditions in the gas phase allow for collisions between different molecules, a factor that has not been taken into account by the theoretical simulation. In addition, the presence of O_2 or N_2 in the experiment might additionally affect the ratio.

cis-Pinonic acid: Simulation of the photolysis of *cis*-pinonic acid (PA) not only predicts Norrish type I and Norrish type II reactions but also two other processes: ring opening and the loss of the $^{\bullet}C(O)OH$ group (decarboxylation). Table 1.2 summarizes the yields of each reaction channel in the simulation of PA at 300 K.

Figure 1.6 shows the snapshots of MD trajectories taken shortly after the different reactions took place in the bare PA molecule.

The following types of events were observed in the simulation of PA. (i) About one-third of the simulations show no reaction even after 100 ps simulation time. (ii) An H atom transfer from methyl group to the carbonyl group (Figure 1.6a), the initial step in Norrish type II reaction, occurred in some trajectories. There was no clear preference for early versus late timing of this event in the simulation time of up to 100 ps. (iii) Loss of $CH_3C(O)^{\bullet}$radical corresponding to Norrish

TABLE 1.2
MD-Simulated Reaction Yields in *cis*-Pinonic Acid

Events	PA 300 K (%)
No reaction	31
Norrish type II reaction (H transfer)	10
Norrish type I reaction (loss of $^{\bullet}CH_3C(O)$)	37
Ring opening	10
Loss of $^{\bullet}C(O)OH$ (decarboxylation)	12

Percentage of total trajectories for a certain reaction channel in 100 ps are listed here.

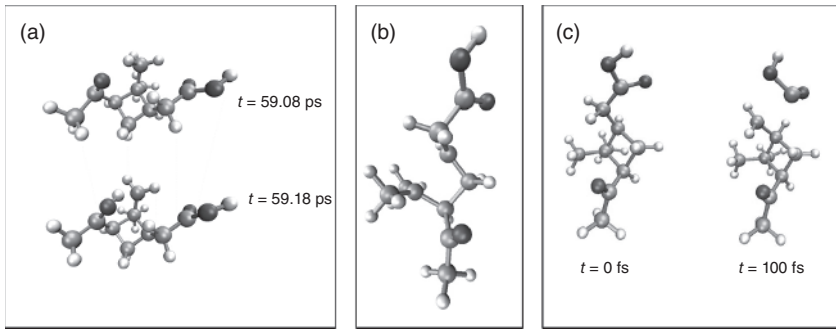

Figure 1.6 *Cis*-pinonic acid: Representative snapshots of MD trajectories taken shortly after the following reactions took place: (a) H-transfer to CO group, (b) opening of the four-membered ring, and (c) decarboxylation. Reproduced with permission from Ref. [33]. Copyright 2013 American Chemical Society.

type I reaction was the most frequently encountered reaction pathway. Its occurrence also was distributed throughout the entire 100 ps window. (iv) A significant number of trajectories culminated in the opening of the cyclobutyl ring (Figure 1.6b). This pathway is ultrafast and its timescale in all the trajectories is less than 20 fs. (v) Decarboxylation, that is, the loss of $^{\bullet}C(O)OH$ from PA, as shown in Figure 1.6c, was observed in some trajectories. In all cases, this process is ultrafast and occurred within 500 fs. All the computed reaction channels have been observed also experimentally [35]. The only process that has not been detected in the experiment is decarboxylation.

1.3.3 Hydrogen Detachment

Pentanal: H detachment in pentanal (see Figure 1.7) is a rare process, as can be seen in Table 1.1.

Also experimentally this pathway is described as a minor fragmentation pathway for aldehydes. The timescale of this process is ultrafast (around 25 fs). Estimates for H detachment in heptanal [14] ranges from 6.9 to 17.8 kcal/mol

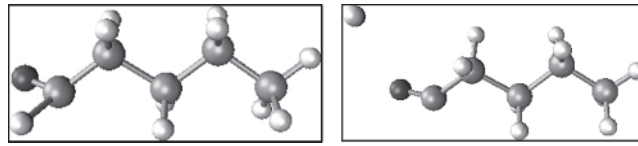

Figure 1.7 H detachment of pentanal. Reprinted with permission from Ref. [31]. Copyright (2013) American Chemical Society.

depending on the specific H detached. The barrier for the H detachment observed here has not been calculated. From the simulation of the bare pentanal, this reaction seems to be a very rare event. However, in the simulation of the cluster, it will turn out to be very important. The discussion of the involvement of H transfer in the cross-molecular reactions is provided in Section 1.3.5.

Pinonic acid: H detachment in pinonic acid has not been observed.

1.3.4 Solvation Effect on Norrish Type Reactions in Pinonic Acid

Table 1.3 provides the reaction yields of methylated pinonic acid with one/five water molecules at 300 K. Although this section mainly focuses on Norrish type I and Norrish type II reactions, the percentage of other reaction channels are given for completeness.

Comparing the yields for the different reaction channels of bare PA with hydrated PA, it can be seen that there is a change in the distribution of the yields of different channels. However, there is no clear trend on the yields as a function of the number of water molecules. This is also observed experimentally: the experiment shows no significant photolysis suppression by the solvent.

1.3.5 Photochemistry in Molecular Aggregates

Finally, we would like to discuss the effect of molecular aggregates on the photochemistry of pentanal. As discussed already earlier, a cluster of five pentanal

TABLE 1.3
The MD-Simulated Reaction Yields in the PAMe-H_2O and PAMe-$(H_2O)_5$ Systems

Events	PAMe-H_2O (%)	PAMe-$(H_2O)_5$ (%)
No reaction/water evaporation	68	39
Norrish type II (H transfer)	2	3
Norrish type I (loss of $CH_3C(O)$)	18	24
Ring opening	5	18
Loss of $^{\bullet}C(O)OCH_3$ (in analogy to the decarboxylation event in bare PA)	6	16

molecules was chosen (Figure 1.1b). It turns out that the cluster has a large effect on the photochemistry of pentanal in the timescale of up to 100 ps. Basically, no different reaction channels were observed than in the bare pentanal, namely, Norrish type I and type II reactions and H-detachment. However, the existence of additional pentanal molecules has an additional impact on the dynamics. For example, the H detachment reaction in the bare pentanal molecule leads to the creation of two fragments, which departs from each other. Here, the H detached can further react with other pentanal molecules and by this lead to the creation of new products. All the reactions observed are a combination of the above-mentioned reactions of the bare pentanal molecule. In the molecular dynamics simulations, up to three subsequent reactions were observed in one trajectory in the timescale of 100 ps. Nine different reaction channels have been observed, which are summarized in Ref. [32] and not repeated here. Out of this, the reaction channels that involve only one single molecule (monomeric reactions) are as follows: (i) First step of the Norrish type I reaction (C—C_α cleavage) in 9% of the trajectories. (ii) γ-H transfer as the first step of Norrish type II reaction in about 1% of the trajectory. (iii) H detachment is observed in 5% of the trajectories.

The statistics of Norrish type I and Norrish type II reactions occurring *in one pentanal molecule in the cluster* (i.e., not followed by subsequent reactions) can be compared with the previously discussed statistics in the bare pentanal, in *cis*-pinonic acid, and hydrated *cis*-pinonic acid: Norrish type I reaction is most pronounced in *cis*-pinonic acid, with 37% of yield, much more than for the bare pentanal (14% only). The water and the pentanal cluster reduce in both systems the percentage of Norrish type I reaction (PA-H_2O – 18%, PA-$(H_2O)_5$ – 24%, pentanal cluster – 9%). On the contrary, Norrish type II reaction is mostly observed in the bare pentanal (27%), compared to 10% for the bare pinonic acid. Hydration of the *cis*-pinonic acid further reduces the percentage of Norrish type II reactions. The existence of the pentanal cluster also decreases the percentage of Norrish type II reaction (PA-H_2O – 2%, PA-$(H_2O)_5$ – 3%, pentanal cluster – 1%).

In addition, for the pentanal cluster, all other reaction channels observed start with either Norrish type I, Norrish type II or H detachment reactions, but continue then further, yielding reactions between different pentanal molecular, so-called cross-molecular reactions. Especially, the H detachment step is noteworthy. In the bare pentanal molecule, this pathway was observed in only 1% of the trajectories. Here, it is involved in most of the trajectory as one of the observed steps of cross-molecular reactions.

As an example of a cross-molecular reaction channel, Figure 1.8 shows one trajectory involving several different reactions.

The first step promptly occurring in about 0.36 ps is the C—C_α cleavage. Some 50 ps later, a favorable configuration is found to enable the H atom transfer from the CHO group to the butyl radical, forming butane and a pentanoyl radical. A third pentanal at about 89.4 ps loses its H atom to the formyl radical resulting in formaldehyde and another pentanoyl radical.

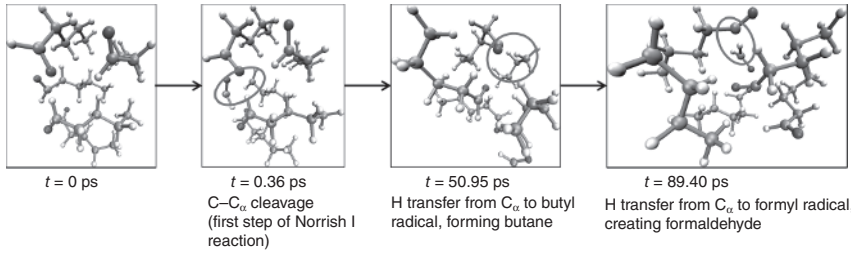

Figure 1.8 Pentanal cluster: Snapshots of one trajectory showing several subsequent reactions. Reproduced from Ref. [32] with permission from the PCCP Owner Societies. *(See color plate section for the color representation of this figure.)*

Dividing the total reaction channels into monomeric and cross-molecular reactions, it is found that about 73% of the reaction channels involve cross-molecular reactions, compared to only 27% of monomeric reactions. The conclusion that follows from these numbers is that the molecular aggregate has a large effect on the photochemistry of pentanal and that it yields a much larger number of different products. It is predicted that longer simulation timescales or larger clusters will even more increase the cross-molecular reactions. Experimental evidences provided in the same Ref. [32] support most of the predicted reaction channels.

Figure 1.9 summarizes using a histogram the timescales observed in the unimolecular reactions in both bare pentanal and pentanal clusters, compared with the timescales of cross-molecular reactions in the pentanal cluster.

The unimolecular reactions observed in the bare pentanal molecule occur almost uniformly over the whole timescale of 100 ps. In contrast, the same unimolecular reactions in the pentanal cluster are much more pronounced in the beginning of the simulation time window. This suggests that unimolecular reactions can only prevail if the excited molecule is optimally oriented at the beginning of the simulation; if it is not, cross-reactions become more probable.

The orientation of the molecules has a large effect on the reactions observed here. Only certain orientations allow an H atom transfer to neighboring molecules. In addition, the cross-molecular processes, especially Norrish type I reaction, are less affected by the initial orientation of the molecules. The cross-reactions observed in the cluster are distributed almost equally over the whole simulation timescale.

1.4 CONCLUDING REMARKS

In this chapter, we applied classical dynamics carried out "on-the-fly" for semiempirical potential energy surfaces to the study of an important family of organic reactions. Only limited experimental data is available for the processes studied,

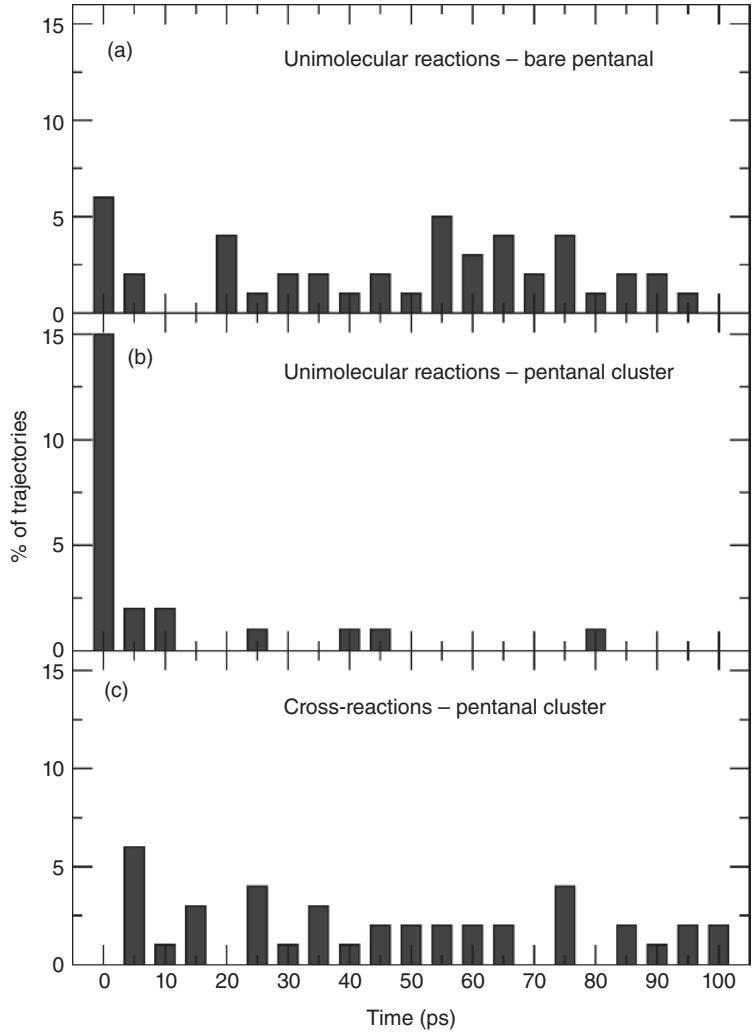

Figure 1.9 Histogram of the (a) number of unimolecular processes in a bare pentanal molecule versus time, (b) unimolecular processes of a pentanal molecule embedded in the pentanal cluster versus time, and (c) cross-reactions in the pentanal cluster versus time. Reproduced from Ref. [32] with permission from the PCCP Owner Societies.

yet tentatively it seems that the point of agreement found strongly encourages the approach of semiempirical molecular dynamics (SEMD) for such photochemical reactions. The limited experimental data that is available seems to be in agreement with the computational approach. The computational approach has the power of prediction that should be tested against future experiments, and which suggest surprising properties of the Norrish type processes investigated here. The fact

that the approach enables the running of relatively long timescale trajectories and furthermore computing many trajectories for meaningful statistics on the reaction products is an essential requirement of any dynamical simulation approach. At least for the more complex examples presented here, such as the clusters of medium-size organic carbonyls, the SEMD simulations proposed here may be the only realistic option at present.

The semiempirical method employed here treats the singlet and triplet potential energy surfaces (both in the ground state and the excited state) correctly at least at the qualitative level. This has been verified in all the systems depicted here by comparing structures and energies with higher level quantum chemical methods. We therefore strongly recommend the usage of the OM2 and OM2/MRCI methods for the photochemistry of organic molecules.

We focused here on triplet-state reactions occurring after photoexcitation. We have not treated the ISC event rigorously, and believe, subject to the evidences provided above, that the ISC event itself is of minor interest in these systems. However, there exist systems where the ISC itself plays an important role. Recent advances in method developments have provided a tool for treating intersystem crossing events. Worthwhile to mention is the work of Gonzalez (SHARC) [71] and Thiel and coworkers [72] in treating internal conversion (IC) and ISC events on the same footing.

Future directions using the above-described approach are envisioned: (i) applications to photochemistry in condensed phases: among the possibilities are the simulation of reactions in solvents, reactions in solids and liquids, and aerosols; (ii) applications to reactions of large organic carbonyls, as an extension to the described work here; (iii) studies on different carbonyls such as ketones and carboxylic acids.

In summary, the above methodology proved successful in simulating the photochemistry of carbonylic compounds. Experimental evidences and validation using high-level *ab initio* methods support the results. Further applications are anticipated.

PERSONAL NOTE (BENNY GERBER)

I first met Moshe Shapiro when we were both undergraduates at The Hebrew University of Jerusalem and have remained his friend ever since then. Years later, we began to cooperate in research when we were both on the faculty of the Weizmann Institute, early in our careers. Moshe was one of my very first collaborators, and he greatly influenced my research and scientific outlook. We very frequently had extensive and quite enthusiastic discussions not only on our joint research but on a whole range of scientific issues. The discussions with Moshe were stimulating and thought provoking. He had the gift of sharp analysis, and the perspectives of his comments were broad. Moshe was a deep thinker of formal aspects of theory,

such as subtle points of quantum mechanics, but also had good insights into the chemistry of systems, which helped him provide pragmatic models. Moshe was able to link formal theory to possible computational modeling and both of these aspects to experiment.

My years of cooperation with Moshe at the Weizmann Institute preceded his brilliant work on coherent control. However, the qualities that led him to his highlight work were all there: the sharpness of his thinking, his grasp of formal theory, and the insights into experimental implications. My choice of photochemistry as the topic of my contribution was influenced by his long-term interest in photodissociation and the fact that we had cooperated, among other topics, on photochemistry at surfaces.

I will clearly miss Moshe and the wonderful discussions that I liked so much.

REFERENCES

1. B. J. Finlayson-Pitts and J. N. J. Pitts. *Chemistry of the Upper and Lower Atmosphere*. Academic Press, New York (2000).
2. P. J. Robinson and K. A. Holbrook. *Unimolecular Reactions*. Wiley, New York (1973).
3. R. G. Gilbert and S. C. Smith. *Theory of Unimolecular and Recombination Reactions*. Blackwell, Oxford (1990).
4. M. I. McCarthy, R. B. Gerber and M. Shapiro. Quantum-theory of the photodissociation of IBr adsorbed on an MgO(0 0 1) surface. *J. Chem. Phys.*, **92**: 7708–7715 (1990).
5. R. Atkinson. "Gas-phase tropospheric chemistry of organic-compounds – a review," *Atmos. Environ. Part A – Gen .Top.*, **24**: 1–41 (1990).
6. T. E. Graedel, L. A. Farrow, and T. A. Weber. "Kinetic studies of photochemistry of urban troposphere," *Atmos. Environ.*, **10**: 1095–1116 (1976).
7. D. Grosjean. "Formaldehyde and other carbonyls in Los Angeles ambient air," *Environ. Sci. Tech.*, **16**: 254–262 (1982).
8. B. N. Fu, B. C. Shepler, and J. M. Bowman. "Three-state trajectory surface hopping studies of the photodissociation dynamics of formaldehyde on ab initio potential energy surfaces," *J. Am. Chem. Soc.*, **133**: 7957–7968 (2011).
9. W. H. Fang. "Ab initio determination of dark structures in radiationless transitions for aromatic carbonyl compounds," *Acc. Chem. Res.*, **41**: 452–457 (2008).
10. D. Townsend, S. A. Lahankar, S. K. Lee, S. D. Chambreau, A. G. Suits, X. Zhang, J. Rheinecker, L. B. Harding, and J. M. Bowman. "The roaming atom: straying from the reaction path in formaldehyde decomposition," *Science*, **306**: 1158–1161 (2004).
11. M. N. R. Ashfold and D. R. Glowacki. "Photochemistry: scrambled by the Sun?," *Nat. Chem.*, **3**: 423–424 (2011).
12. B. R. Heazlewood, A. T. Maccarone, D. U. Andrews, D. L. Osborn, L. B. Harding, S. J. Klippenstein, M. J. T. Jordan, S. H. Kable. "Near-threshold H/D exchange in CD(3)CHO photodissociation," *Nat. Chem.*, **3**: 443–448 (2011).
13. J. M. Tadic, G. K. Moortgat, P. P. Bera, M. Loewenstein, E. L. Yates, T. J. Lee. "Photochemistry and photophysics of *n*-butanal, 3-methylbutanal, and 3,3-dimethylbutanal: experimental and theoretical study," *J. Phys. Chem. A*, **116**: 5830–5839 (2012).

14. S. E. Paulson, D. L. Liu, G. E. Orzechowska, L. M. Campos, K. N. Houk. "Photolysis of heptanal," *J. Org. Chem.*, **71**: 6403–6408 (2006).
15. J. M. Tadic, L. Xu, K. N. Houk, and G. K. Moortgat. "Photooxidation of *n*-octanal in air: experimental and theoretical study," *J. Org. Chem.*, **76**: 1614–1620 (2011).
16. T. J. Cronin and L. Zhu. "Dye laser photolysis of n-pentanal from 280 to 330 nm," *J. Phys. Chem. A*, **102**: 10274–10279 (1998).
17. X. B. Chen and W. H. Fang. "Norrish I vs II reactions of butanal: a combined CASSCF, DFT and MP2 study," *Chem. Phys. Lett.*, **361**: 473–482 (2002).
18. L. Zhu, T. Cronin, and A. Narang. "Wavelength-dependent photolysis of i-pentanal and t-pentanal from 280 to 330 nm," *J. Phys. Chem. A*, **103**: 7248–7253 (1999).
19. L. Zhu, Y. X. Tang, Y. Q. Chen, and T. Cronin. "Wavelength-dependent photolysis of C3–C7 aldehydes in the 280–330 nm region," *Spectrosc. Lett.*, **42**: 467–478 (2009).
20. J. Tadic, I. Juranic, and G. K. Moortgat. "Photooxidation of *n*-hexanal in air," *Molecules*, **6**: 287–299 (2001).
21. Y. X. Tang and L. Zhu. "Wavelength-dependent photolysis of *n*-hexanal and n-heptanal in the 280–330-nm region," *J. Phys. Chem. A*, **108**: 8307–8316 (2004).
22. J. M. Tadic, I. O. Juranic, and G. K. Moortgat. "Photooxidation of *n*-heptanal in air: Norrish type I and II processes and quantum yield total pressure dependency," *J. Chem. Soc. Perkin Trans.*, **2**: 135–140 (2002).
23. K. C. Thompson, D. L. Crittenden, S. H. Kable, and M. J. T. Jordan. "A classical trajectory study of the photodissociation of T-1 acetaldehyde: the transition from impulsive to statistical dynamics," *J. Chem. Phys.*, **124**: 044302 (2006).
24. Y. C. Han, B. C. Shepler, J. M. Bowman. "Quasiclassical trajectory calculations of the dissociation dynamics of CH(3)CHO at high energy yield many products," *J. Phys. Chem. Lett.*, **2**: 1715–1719 (2011).
25. M. N. D. S. Cordeiro, E. Martinez-Nunez, A. Fernandez-Ramos, and S. A. Vazquez. "Direct dynamics study of the photodissociation of triplet propanal at threshold," *Chem. Phys. Lett.*, **381**: 37–44 (2003).
26. G. F. Metha, A. C. Terentis, and S. H. Kable. "Near threshold photochemistry of propanal. Barrier height, transition state structure, and product state distributions for the HCO channel," *J. Phys. Chem. A*, **106**: 5817–5827 (2002).
27. Y. Kurosaki. "Energy-flow dynamics in the molecular channel of propanal photodissociation, C2H5CHO -> C2H6+CO: direct ab initio molecular dynamics study," *J. Phys. Chem. A*, **110**: 11230–11236 (2006).
28. M. A. Buntine, C. Lee, G. F. Metha. "The lowest-lying excited singlet and triplet electronic states of propanal: an ab initio molecular orbital investigation of the potential energy surfaces," *Phys. Chem. Chem. Phys.*, **6**: 688–696 (2004).
29. M. J. S. Dewar, C. Doubleday. "Mindo-3 study of Norrish type-II reaction of butanal," *J. Am. Chem. Soc.*, **100**: 4935–4941 (1978).
30. R. R. Sauers and L. A. Edberg. "Modeling of Norrish type-II reactions by semiempirical and ab initio methodology," *J. Org. Chem.*, **59**: 7061–7066 (1994).
31. D. Shemesh, Z. G. Lan, and R. B. Gerber. "Dynamics of triplet-state photochemistry of pentanal: mechanisms of Norrish I, Norrish II, and H abstraction reactions," *J. Phys. Chem. A*, **117**: 11711–11724 (2013).
32. D. Shemesh, S. L. Blair, S. A. Nizkorodov, R. B. Gerber. "Photochemistry of aldehyde clusters: cross-molecular versus unimolecular reaction dynamics," *Phys. Chem. Chem. Phys.*, **16**: 23861–23868 (2014).

33. H. Lignell, S. A. Epstein, M. R. Marvin, D. Shemesh, R. B. Gerber, and S. A. Nizkorodov. "Experimental and theoretical study of aqueous *cis*-pinonic acid photolysis," *J. Phys. Chem. A*, **117**: 12930–12945 (2013).

34. E. K. C. Lee and R. S. Lewis. "Photochemistry of simple aldehydes and ketones in the gas phase," *Adv. Photochem.*, **12**: 1–96 (1980).

35. Y. Kurosaki. "Hydrogen-atom production channels of acetaldehyde photodissociation: direct DFT molecular dynamics study," *J. Mol. Struct. – THEOCHEM*, **850**: 9–16 (2008).

36. G. A. Amaral, A. Arregui, L. Rubio-Lago, J. D. Rodriguez, and L. Banares. "Imaging the radical channel in acetaldehyde photodissociation: competing mechanisms at energies close to the triplet exit barrier," *J. Chem. Phys.*, **133**: 064303 (2010).

37. D. Shemesh, G. M. Chaban, and R. B. Gerber. "Photoionization dynamics of glycine: the first 10 picoseconds," *J. Phys. Chem. A*, **108**: 11477–11484 (2004).

38. F. Jensen. *Introduction to Computational Chemistry*. John Wiley & Sons, Chichester (2007).

39. W. Weber and W. Thiel. "Orthogonalization corrections for semiempirical methods," *Theor. Chem. Acc.*, **103**, 495–506 (2000).

40. A. Koslowski, M. E. Beck, and W. Thiel. "Implementation of a general multireference configuration interaction procedure with analytic gradients in a semiempirical context using the graphical unitary group approach," *J. Comput. Chem.*, **24**: 714–726 (2003).

41. S. A. Epstein, D. Shemesh, V. T. Tran, S. A. Nizkorodov, and R. B. Gerber. "Absorption spectra and photolysis of methyl peroxide in liquid and frozen water," *J. Phys. Chem. A*, **116**: 6068–6077 (2012).

42. D. Shemesh and R. B. Gerber. "Femtosecond timescale deactivation of electronically excited peroxides at ice surfaces," *Mol. Phys.*, **110**: 605–617 (2012).

43. D. Shemesh and R. B. Gerber. "Classical trajectory simulations of photoionization dynamics of tryptophan: intramolecular energy flow, hydrogen-transfer processes and conformational transitions," *J. Phys. Chem. A*, **110**: 8401–8408 (2006).

44. D. Shemesh and R. B. Gerber. "Different chemical dynamics for different conformers of biological molecules: photoionization of glycine," *J. Chem. Phys.*, **122**: 241104 (2005).

45. D. Shemesh, R. Baer, T. Seideman, and R. B. Gerber. "Photoionization dynamics of glycine adsorbed on a silicon cluster: "On-the-fly" simulations," *J. Chem. Phys.*, **122**: 184704 (2005).

46. Y. Miller, G. M. Chaban, B. J. Finlayson-Pitts, R. B. Gerber. "Photochemical processes induced by vibrational overtone excitations: dynamics simulations for *cis*-HONO, *trans*-HONO, HNO(3), and HNO(3)-H(2)O," *J. Phys. Chem. A*, **110**: 5342–5354 (2006).

47. Y. Miller and R. B. Gerber. "Dynamics of vibrational overtone excitations of H(2)SO(4), H(2)SO(4)-H(2)O: hydrogen-hopping and photodissociation processes," *J. Am. Chem. Soc.*, **128**: 9594–9595 (2006).

48. M. Shmilovits-Ofir, Y. Miller, and R. B. Gerber. "Conformational transitions of glycine induced by vibrational excitation of the O–H stretch," *Phys. Chem. Chem. Phys.*, **13**: 8715–8722 (2011).

49. M. Shmilovits-Ofir, R. B. Gerber. "Proton transfer and dissociation of GlyLysH(+) following O–H and N–H stretching mode excitations: dynamics simulations," *J. Am. Chem. Soc.*, **133**: 16510–16517 (2011).

50. C. Møller and M. S. Plesset. "Note on an approximation treatment for many-electron systems," *Phys. Rev.*, **46**: 618–622 (1934).

51. T. H. Dunning. "Gaussian-basis sets for use in correlated molecular calculations. 1. The atoms boron through neon and hydrogen," *J. Chem. Phys.*, **90**: 1007–1023 (1989).

52. F. Weigend and M. Haser. "RI-MP2: first derivatives and global consistency," *Theor. Chem. Acc.*, **97**: 331–340 (1997).

53. J. Schirmer. "Beyond the random-phase approximation – a new approximation scheme for the polarization propagator," *Phys. Rev. A*, **26**: 2395–2416 (1982).

54. W. Thiel. MNDO program, version 6.1, Mülheim an der Ruhr, Germany (2007).

55. J. C. Tully. "Molecular-dynamics with electronic-transitions," *J. Chem. Phys.*, **93**: 1061–1071 (1990).

56. J. G. Calvert and J. N. Pitts. *Photochemistry*. John Wiley, New York (1966).

57. M. Korth and W. Thiel. "Benchmarking semiempirical methods for thermochemistry, kinetics, and noncovalent interactions: OMx methods are almost as accurate and robust as DFT-GGA methods for organic molecules," *J. Chem. Theory Comput.*, **7**: 2929–2936 (2011).

58. E. Fabiano and W. Thiel. "Nonradiative deexcitation dynamics of 9H-adenine: an OM2 surface hopping study," *J. Phys. Chem. A*, **112**: 6859–6863 (2008).

59. Z. G. Lan, E. Fabiano, and W. Thiel. "Photoinduced nonadiabatic dynamics of pyrimidine nucleobases: on-the-fly surface-hopping study with semiempirical methods," *J. Phys. Chem. B*, **113**: 3548–3555 (2009).

60. Z. G. Lan, E. Fabiano, and W. Thiel. "Photoinduced nonadiabatic dynamics of 9H-guanine," *Chemphyschem*, **10**: 1225–1229 (2009).

61. Y. Lu, Z. G. Lan, and W. Thiel. "Hydrogen bonding regulates the monomeric nonradiative decay of adenine in DNA strands," *Angew. Chem., Int. Ed.*, **50**: 6864–6867 (2011).

62. A. Kazaryan, Z. G. Lan, L. V. Schafer, M. Filatov, and W. Thiel. "Surface hopping excited-state dynamics study of the photoisomerization of a light-driven fluorene molecular rotary motor," *J. Chem. Theory Comput.*, **7**: 2189–2199 (2011).

63. O. Weingart, Z. G. Lan, A. Koslowski, and W. Thiel. "Chiral pathways and periodic decay in *cis*-azobenzene photodynamics," *J. Phys. Chem. Lett.*, **2**: 1506–1509 (2011).

64. Z. G. Lan, Y. Lu, E. Fabiano, W. Thiel. "QM/MM nonadiabatic decay dynamics of 9H-adenine in aqueous solution," *Chemphyschem*, **12**: 1989–1998 (2011).

65. P. Strodel and P. Tavan. "A revised MRCI-algorithm coupled to an effective valence-shell Hamiltonian. II. Application to the valence excitations of butadiene," *J. Chem. Phys.*, **117**: 4677–4683 (2002).

66. M. Wanko, M. Hoffmann, P. Strodel, A. Koslowski, W. Thiel, F. Neese, T. Frauenheim, and M. Elstner. "Calculating absorption shifts for retinal proteins: computational challenges," *J. Phys. Chem. B*, **109**: 3606–3615 (2005).

67. M. Hoffmann, M. Wanko, P. Strodel, P. H. Konig, T. Frauenheim, K. Schulten, W. Thiel, E. Tajkhorshid, M. Elstner. "Color tuning in rhodopsins: the mechanism for the spectral shift between bacteriorhodopsin and sensory rhodopsin II," *J. Am. Chem. Soc.*, **128**: 10808–10818 (2006).

68. M. R. Silva-Junior, M. Schreiber, S. P. A. Sauer, and W. Thiel. "Benchmarks of electronically excited states: basis set effects on CASPT2 results," *J. Chem. Phys.*, **133**: 174318 (2010).

69. M. R. Silva-Junior and W. Thiel. "Benchmark of electronically excited states for semiempirical methods: MNDO, AM1, PM3, OM1, OM2, OM3, INDO/S, and INDO/S2," *J. Chem. Theory Comput.*, **6**: 1546–1564 (2010).

70. J. Tadic, I. Juranic, G. K. Moortgat. "Pressure dependence of the photooxidation of selected carbonyl compounds in air: *n*-butanal and *n*-pentanal," *J. Photochem. Photobiol. A: Chem.*, **143**: 169–179 (2001).

71. M. Richter, P. Marquetand, J. Gonzalez-Vazquez, I. Sola, and L. Gonzalez. "SHARC: ab initio molecular dynamics with surface hopping in the adiabatic representation including arbitrary couplings," *J. Chem. Theory Comput.*, **7**: 1253–1258 (2011).

72. G. L. Cui and W. Thiel. "Generalized trajectory surface-hopping method for internal conversion and intersystem crossing," *J. Chem. Phys.*, **141** (2014).